Energetics of hydrogen coverage on group VIII transition metal surfaces and a kinetic model for adsorption/desorption

Francesco Faglioni[a)]
Dipartimento di Chimica, Università degli Studi, Via G. Campi 183, 41100 Modena, Italy

William A. Goddard III[b)]
Materials and Process Simulation Center (139-74), California Institute of Technology, Pasadena, California 91125

We determined the binding energy of hydrogen to the closest packed surface for all nine group VIII transition metals as a function of surface coverage using quantum mechanics (density functional theory with the generalized gradient approximation) with periodic boundary conditions. The study provides a systematic comparison of the most stable surfaces of the nine group VIII transition metals, leading to results consistent with available surface science studies. We then use these to develop a simple thermodynamic model useful in estimating the surface coverage under typical heterogeneous catalysis conditions and compare these results to temperature programmed desorption experiments. © *2005 American Institute of Physics.* [DOI: 10.1063/1.1814938]

I. INTRODUCTION

Many of the group VIII transition metals play an important role in industrially important heterogeneous catalysts for a broad range of hydrocarbon transformations.[1,2] Consequently the behavior of their surfaces has been object of intense study for several decades using techniques ranging from surface science studies in ultrahigh vacuum to kinetic studies to theoretical simulations. However, due to the complexity of heterogeneous reactions under catalytic conditions, there remains considerable uncertainty regarding the chemical behavior of the surface. Indeed even the nature of the simplest adsorbates is not well characterized. In particular, a central role in hydrocarbon reactions and rearrangements on surfaces is played by the behavior of hydrogen under reaction conditions of temperature and pressure, but it is difficult to obtain either experimental or theoretical predictions for these reaction conditions. Indeed even a systematic comparison for different metals is hampered by the wide range of techniques and coverage conditions used by the various groups. Reviews of hydrogen chemistry on transition metal surfaces are available in the literature.[3–5]

In this paper we report consistent computational studies of hydrogen adsorption on the most stable surfaces of all nine group VIII transition metals. The aim of the study is to provide a systematic comparison of the hydrogen binding energy on the surfaces considered at varying levels of coverage in order to provide a consistent set of results to be used in interpreting both catalysis experiments and surface science studies. Although subsurface hydrogen may participate in some surface reactions, we consider here only surface adsorption.

In Sec. II we describe the computational details and the main approximations used with an estimate of the error bars associated with our result. In Sec. III we report the computed binding energies and geometries and compare with available results from other groups. In Sec. IV we discuss our results in terms of three simple statistical thermodynamics treatments of the adsorbed hydrogen. Specific examples are provided in the case of Ir to illustrate a comparison with surface science results. Here, we also review the experimental literature and compare to our predictions where possible.

II. COMPUTATIONAL DETAILS

A. Quantum mechanics

We used the generalized gradient approximation (GGA) density functional developed by Perdew and Wang[6] with a periodic plane-wave basis set to describe the wave function. All computations were performed using CASTEP (Ref. 7) via the CERIUS2 interface.[8] Recpot[9] effective core potential (ECP) was used on all metal atoms and Troullier–Martins ECP (Refs. 10 and 11) on hydrogen, as implemented in CASTEP. The cutoff energy for plane wave expansion was set at 600 eV for all systems. This value was selected according to recommendations for the ECPs and is expected to provide consistently good quality results. We kept the cutoff constant for all nine systems to simplify comparison of numerical results.

B. Surface calculations

All metal atoms were held fixed at the experimental bulk geometry with only the position of the adsorbed hydrogen optimized. Based on our testing and on published results[12,13] we expect relaxation to affect binding energies by up to 2 kcal/mol. We did not consider subsurface adsorption.

We carried out calculations on platinum and iridium surfaces for various number of layers in the slab and found reasonable convergence in the hydrogen binding energy and equilibrium geometry starting at four layers. Specifically,

---
[a)]Electronic mail: cecco@unimo.it
[b)]Electronic mail: wag@wag.caltech.edu

adding a fifth layer changed the hydrogen binding energy by less than 0.3 kcal/mol for Ir and 0.1 kcal/mol for Pt. Hence, we adopted a four-layer slab for all metallic surfaces. For the vacuum between slabs we used an interlayer distance equivalent to six layers at the bulk geometry (five layers of vacuum). Hydrogen was allowed to adsorb only on one side of the slab.

For the surface unit cells (SUC) we used both 1×1 and $\sqrt{3}\times\sqrt{3}\,R(30°)$. The convergence of the total energy and the binding energy with the number of k points was tested in the case of Pt(111) with 1×1 SUC. We found that a 12×12 Monkhorst–Pack grid in the plane of the surface yields energies within 0.016 eV (0.38 kcal/mol) of the value obtained with the 20×20 grid. Hence we used the 12×12 Monkhorst–Pack grids on 1×1 SUC. Accordingly, for the $\sqrt{3}\times\sqrt{3}\,R(30°)$ SUC we used the 7×7 grids. One k point was used for the direction normal to the surface.

Spin polarization of the wave function was not allowed. We tested the magnitude of this approximation by computing the fcc H binding energy on Ni(111) at monolayer (ML) coverage both with and without spin polarization. Due to software restrictions, to perform this task we used ultrasoft potentials[14] with core correction on the metals and an energy cutoff of 340 eV. The computed values are 67.8 and 66.2 kcal/mol with and without spin polarization, respectively. The effect of spin polarization is thus of 1.6 kcal/mol, which is smaller than the error bar associated with the choice of the ECP (*vide infra*).

C. Kinetics simulations

Adsorption and desorption kinetics simulations were performed by numerical integration of the Eqs. (36), (38), and (39). All simulated kinetics proved independent from the numerical integration technique used provided that sufficiently small time steps were used. The results reported were obtained with standard fourth-order Runge-Kutta equations using variable time steps. The initial time step was set at 0.01 s. The software used to do these simulations is available in the supplementary material.

III. RESULTS

In order to understand hydrogen binding to closest packed surfaces, it is essential to establish the binding geometry and to estimate the barrier for surface diffusion. To study this we used the 1×1 SUC to compute hydrogen binding energy (BE) at different surface sites for ML coverages. We then selected the most stable sites to investigate how the BE depends on coverage.

The computed hydrogen BE and equilibrium distance from the surface for the high symmetry positions on the closest packed surfaces considered are reported in Table I. In the case of Fe and Co, we considered both the phases found at room temperature and pressure (bcc and hcp, respectively) and the two closest packed phases stable under more drastic conditions (fcc). To compute the BE, we assumed the energy of gas phase hydrogen to be the exact value for the Hamiltonian used, i.e., -0.5 hartree ($-13.605\,70$ eV). The BE reported in Table I do not include zero point energy (ZPE)

TABLE I. Computed hydrogen binding energy to metal surfaces at different surface sites. The data refer to 1 ML coverage. See text for computational details.

Surface	Site	D_e (kcal/mol)	Height (Å)
Fe-bcc (110)	cap	65.3	0.981
	bridge1	60.7	0.968
	bridge2	61.3	1.192
	top	48.1	1.577
Fe-fcc (111)	fcc	67.1	0.972
	hcp	66.5	0.961
	top	46.4	1.573
	bridge	61.3	1.124
Ru-hcp (001)	fcc	61.8	1.090
	hcp	61.7	1.079
	top	49.7	1.652
	bridge	58.0	1.233
Os-hcp (001)	fcc	62.2	1.081
	hcp	61.3	1.077
	top	60.1	1.638
	bridge	60.9	1.223
Co-hcp (001)	fcc	61.3	1.009
	hcp	60.3	0.990
	top	45.2	1.551
	bridge	56.6	1.139
Co-fcc (111)	fcc	61.6	0.999
	hcp	60.9	0.997
	top	45.2	1.560
	bridge	56.9	1.138
Rh-fcc (111)	fcc	58.7	1.042
	hcp	57.7	1.021
	top	49.6	1.616
	bridge	55.8	1.184
Ir-fcc (111)	fcc	60.4	1.040
	hcp	59.2	1.035
	top	61.8	1.587
	bridge	59.6	1.171
Ni-fcc (111)	fcc	60.9	0.955
	hcp	60.1	0.962
	top	44.1	1.525
	bridge	55.9	1.090
Pd-fcc (111)	fcc	59.3	0.918
	hcp	57.4	0.891
	top	45.7	1.594
	bridge	54.1	1.088
Pt-fcc (111)	fcc	58.7	0.957
	hcp	56.9	0.953
	top	58.5	1.580
	bridge	57.4	1.105

corrections due to the vibrational motion of the adsorbed atoms. We expect this correction to be approximately the same for fcc and hcp sites on the same metal and somewhat larger for top sites. For all closest packed (fcc and hcp) metals, we calculate that adsorption at the fcc site is favored with respect to the hcp site and, except for Ru, the difference is about 1–2 kcal/mol, indicating that fcc is the preferred site at ML coverage. For Ru the difference between fcc and hcp is

TABLE II. Hydrogen binding energy and vibrational frequency on metal surfaces at different surface coverages. D_e indicates the electronic binding energy in kcal/mol [no corrections from zero point vibrational energy (ZPE)]. The frequency ν refers to the symmetric stretching normal to the surface and is expressed in cm^{-1}. D_0 is the ZPE corrected value in kcal/mol obtained from D_e and ν. Values in parentheses are estimates obtained as described in the text.

Coverage	Metal	Site	D_e	ν	D_0	Metal	Site	D_e	ν	D_0	Metal	Site	D_e	ν	D_0
1/3 ML		cap	68.1	1069	64.6		fcc	62.4	1235	60.6		fcc	62.0	1168	60.3
2/3 ML	Fe	cap	65.1	(1101)	(63.5)	Co	fcc	60.7	(1276)	(58.9)	Ni	fcc	60.6	(1225)	(58.9)
1 ML	bcc		64.7	1133	63.1	hcp		60.3	1317	58.4	fcc		60.1	1282	58.3
4/3 ML		cap, cap	40.1	⋯	(38.5)		fcc, hcp	35.3	⋯	(33.4)		fcc, hcp	36.3	⋯	(34.5)
1/3 ML		fcc	67.8	1237	66.0		fcc	62.5	1184	60.8					
2/3 ML	Fe	fcc	66.8	(1216)	(65.1)	Co	fcc	61.3	(1252)	(59.5)					
1 ML	fcc		66.6	1196	64.9	fcc		60.7	1320	58.8					
4/3 ML		fcc, hcp	39.9	⋯	(38.2)		fcc, hcp	36.0	⋯	(34.1)					
1/3 ML		hcp	62.6	1154	61.0										
2/3 ML		hcp	61.3	(1202)	(59.6)										
1 ML			60.7	1251	58.9										
1/3 ML	Ru	fcc	63.4	1119	61.8			59.5	1151	57.9			60.2	1146	58.6
2/3 ML	hcp	fcc	61.7	(1127)	(60.1)	Rh	fcc	58.9	(1229)	(57.1)	Pd	fcc	59.4	(1090)	(57.8)
1 ML			60.5	1135	58.9	fcc		58.5	1308	56.6	fcc		57.5	1035	56.0
4/3 ML		fcc, hcp	36.2	⋯	(34.6)		fcc, hcp	37.6	⋯	(35.7)		fcc, hcp	34.7	⋯	(33.2)
1/3 ML							top	63.0	2345	59.7					
2/3 ML							top	62.4	(2339)	(59.1)					
1 ML								62.0	2333	58.7					
1/3 ML	Os	fcc	64.9	1177	63.2	Ir	fcc	61.5	1244	59.7		fcc	59.9	1155	58.3
2/3 ML	hcp	fcc	62.7	(1183)	(61.0)	fcc	fcc	60.8	(1267)	(59.0)	Pt	fcc	59.3	(1164)	(57.6)
1 ML			61.4	1189	59.7			60.1	1290	58.3	fcc		58.4	1173	56.7
4/3 ML		top, fcc	53.1	⋯	(46.6)		top, fcc	56.2	⋯	(54.4)		top, fcc	49.2	⋯	(45.9)

only 0.1 kcal/mol so that ZPE corrections would be needed to determine which of the two sites is more stable. Except for third row metals, the top position is considerably less favorable than either fcc or hcp. For Ir, we find that the top position is 1.4 kcal/mol more stable than fcc. We expect the ZPE correction to be larger for top adsorption positions than for either fcc or hcp so we considered both adsorption geometries for further investigations on the larger SUC.

Our conclusion is that fcc geometry is favored on all metals with the possible exceptions of Ru, where hcp is equally favored, and Ir, where top may be equally favored.

Based on experimental results for several metals and on previous calculations, we expect the barrier for surface diffusion of hydrogen to be relatively small. To verify this assumption, we computed the energy for the bridge position between fcc and hcp sites on all the closest packed surfaces considered. In the case of Fe-bcc (110) there are two distinct bridge positions between equivalent cap sites. Although the bridge position is not the exact transition state and despite the fact that we used ML coverage, the energy of the bridge position provides an estimate of the barrier for surface diffusion. We thus estimate this barrier to be around 5 kcal/mol for Fe, Co, and Ni, around 3 to 5 kcal/mol for Ru, Rh, and Pd, and close to 1 or 2 kcal/mol for Os, Ir, and Pt. In the case of Ir and Pt, the bridge position has lower energy than the hcp.

We used the $\sqrt{3} \times \sqrt{3}\,R(30°)$ SUC to calculate the coverage dependence of the BE for the most stable positions. This is suitable for 1/3, 2/3, and 3/3 ML coverages and for coverages past 1 ML. Although on certain metal surfaces, most notably Ni(111) (Ref. 15) and Fe(110) (Refs. 15 and 16) there is evidence of adsorption at different sites for coverages near 1/2 ML at low temperature, probably due to an overall minimization of adsorbates interaction, we found that for the coverages of 1/3 and 2/3 ML the most stable adsorption geometry comprises pure fcc sites. A more detailed description of the hydrogen behavior at various coverages and on specific metals is beyond the scope of this article. We refer the interested reader to the literature regarding specific metal surfaces.[15] The computed BEs are reported in Table II. We find that for all systems there is a gradual decrease in the BE going from 1/3 ML to 1 ML by an average of 2.0 kcal/mol out of 61.6 or 3.2%. The largest changes (≈3 kcal/mol) were for Os, Pd, and Ru. The smallest changes (≈1 kcal/mol) were for Ir on-top, Rh, and Fe fcc.

To investigate coverage past 1 ML, we studied all plausible adsorption configurations corresponding to 4/3 ML for the third row metals. We report in Table II the most stable configuration. For first and second row elements we only considered adsorption in the cap positions (1 ML fcc and 1/3 ML hcp). Going from 1 ML to 4/3 ML coverage leads to a large drop (10–30 kcal/mol) in binding energy for all systems except Ir. For Ir, the binding energy decreases only by 5.8 kcal/mol. Since the H–H bond strength is 110 kcal/mol, a bond strength of less than 55 kcal/mol will lead to a state unstable with respect to desorption. With the possible exception of Ir, the binding energy for 4/3 ML is generally too low to allow a significant population of this state in equilibrium with gas phase H_2 even under very drastic conditions. A more detailed discussion of adsorption on Ir is reported in Sec. IV.

In order to compare our binding energies D_e to experimental data, we corrected for the ZPE vibrational mode perpendicular to the surface. We computed the harmonic fre-

TABLE III. Comparison of computed and experimental data. Values for D_0 are reported for 1/3 ML coverage to compare with experimental values at low coverage. The range of computed frequencies is given by the 1/3 ML and 1 ML values. The last column contains the references used for the experimental results.

Surface	D_0 (kcal/mol)		ω (cm^{-1})		References
	Comp.	Expt.	Comp.	Expt.[a]	
Fe-bcc (110)	64.6	64.8	1069–1133	1060	3
Co-hcp (001)	60.6	59.8	1235–1317		3
Ni-fcc (111)	60.3	63.1	1168–1282	1170	3, 17
Ru-hcp (001)	61.8	61.2–66.0	1119–1135	1112–1136	3
Rh-fcc (111)	57.9	60.9	1151–1308	1088–1100	3, 18
Pd-fcc (111)	58.6	62.1	1035–1146	998	3
Ir-fcc (111)	59.7	58.1	2333–2345	2030	3, 19
Pt-fcc (111)	58.3	56.6–60.9	1155–1173	1230	3

[a]Most experimental measurements are based on HREELS with typical accuracy of 8 meV=65 cm^{-1}.

quencies for this vibrational mode for 1/3 and 3/3 ML coverages using numerical differentiation. The frequencies are reported in Table II. The frequency for 2/3 ML coverage was estimated as the average of the 1/3 and 3/3 ML values. These frequencies were used to correct for vibrational zero point energy for coverages up to 1 ML, leading to the D_0 BE in the last column of Table II. The ZPE at 4/3 ML was estimated by assuming that the correction for hcp sites is the same as for fcc sites at 1 ML and the correction for all top sites is the same as computed for the top position on Ir at 1 ML coverage. The D_0 values are the finite-difference BEs at 0 K, i.e., the energies gained by adding one third of a monolayer and represent an estimate to the differential BEs measured experimentally. As the diffusion barriers are low, the motion parallel to the surface is expected to give negligible contributions to the ZPE and to be highly anharmonic. This motion is included in the statistical treatment reported later in this article but it is neglected in the present comparison of low temperature binding energies.

Our results refer to unrelaxed defect-free surfaces. We investigated the effect of surface relaxation in the case of Pt by relaxing the first two metal layers. In this case, the hydrogen binding energy increases by 1.2, 0.3, and 0.7 kcal/mol for 1/3, 2/3, and 3/3 ML coverages, respectively. The average increase of 0.7 kcal/mol is comparable with the expected accuracy of the computational method.

IV. DISCUSSION

A. Comparison of binding energies and vibrational frequencies with experiment

The binding energies D_0 and symmetric vibrational frequencies ν reported in Table II are compared with published experimental values in Table III.

Since most experimental BEs refer to low coverage extrapolations, we compare them with the computed values for 1/3 ML. Experimental frequencies are typically measured near ML coverage. The values we compute for ML coverage, however, neglect the coupling between vibrational motion of neighboring atoms and is thus somewhat approximate. Fortunately, the computed coverage dependent frequency shift is

small and even large relative errors in the frequencies will have small effects on thermodynamics predictions. To compare with the experimental frequencies we report in Table III the computed values for both 1/3 ML and 1 ML, as an estimate of the computational range.

The uncertainty in the experimental binding energies seems to be 4–5 kcal/mol based on the results reported for Pt and Ru. For these systems, the calculated values are within the range of experimental results. For the other six systems (we found no experimental results for Os), the mean average discrepancy is 2.0 kcal/mol.

The computed frequencies are within experimental uncertainty of experiment for Fe, Ni, and Ru, high by 5% for Rh and Pd, low by 6% for Pt, and high by 16% for Ir (on top).

B. Comparison to previous calculations

Several detailed computational investigations have been published focusing on one or a few particular metal surfaces. Since it is beyond the scope of this article to provide a complete review of published results, we report only a few of the most recent publications in order to assess the quality of the binding energies we report. We refer the reader to the cited papers for more exhaustive references relative to specific metal surfaces.

The most systematic calculations of hydrogen chemisorption on metal surfaces are by Nordlander et al.,[20] using effective medium theory. However, this work does not address the binding energy dependence on surface coverage. The results from these studies, reported only in graphical form, range approximately from 62 to 67 kcal/mol over all nine elements. In comparison, for the same surfaces we find the range 59.9–66.1 kcal/mol. The largest discrepancies are for Rh (59.5 versus ≈63 kcal/mol) and Os (64.9 versus ≈67 kcal/mol), with the other values within ≈2 kcal/mol for each surface considered. The trend predicted by Nordlander et al.[20] of decreasing binding energies with increasing atomic number within each row is reproduced by our estimates for 1/3 ML coverage but not for higher coverages.

Hydrogen chemisorption on Fe-bcc(110) was studied by Jiang and Carter[21] (JC), who employed seven layers with a 14×14×1 Monkhorst–Pack grid to perform spin polarized, all electron calculations with relaxed surface. We obtain the same order for the occupation of surface sites, i.e., we find cap to be the most stable site, followed by the two bridge positions and the top site. JC report two values for BEs obtained with different density functionals and our BEs are bracketed by those values both at low and high coverage, i.e., fall within the range 65.3–69.2 kcal/mol for 1/4 ML and 63.6–67.1 kcal/mol for 1 ML. Our computed bond distances to the surface for ML coverage are 0.04–0.08 Å longer than those reported by JC.

Our computed BEs on Ni appear a few kcal/mol smaller than those reported by Greeley and Mavrikakis[22] (GM) and Kresse and Hafner[23] (KH). In fact, both GM and KH report values for D_e of 66.6 and 66.0 (GM) or 65.9 (KH) kcal/mol for 1/4 ML and 1 ML, respectively, versus our values of 62.0 and 60.9 kcal/mol. Although our neglect of surface relaxation and spin polarization may contribute to this difference,

KH estimate these effects at approximately 2–3 kcal/mol. The difference between our results and those reported by GM and KH appears to be due mainly to the choice of different pseudopotentials. As reported in Sec. II, the monolayer BE computed with ultrasoft potentials is 67.8 (without spin polarization) or 66.2 kcal/mol (with spin polarization), in good agreement with GM and KH. As the experimental BE is reported at 63.1 kcal/mol[3] and we estimate the ZPE correction of the order of 1.7 kcal/mol, it is not clear which pseudopotential provides a better description of the binding process.

Our computed BE for H on Ru(001) compares well with the results of Ciobîcă *et al.*[24] and Norskøv and co-workers[25] who report values for D_e in fcc sites at 1/4 ML coverage of 53.5 kJ/mol[2] (Ref. 24) and 0.405 eV (Ref. 25) with respect to gas phase H_2. Assuming a BE for H_2 of 4.58 eV, as computed by KH with a similar potential, we obtain a D_e with respect to atomic H of 65.6 and 62.1 kcal/mol, respectively, which bracket our 63.4 kcal/mol computed for 1/3 ML coverage. Ciobîcă *et al.* also found that the energy difference between fcc and hcp sites is extremely small with the fcc slightly more stable.

Hydrogen chemisorption on Rh(111) was studied with density functional techniques by Mavrikakis *et al.*[26] and Lai.[27] They find BEs (D_e) of 64.3 or 60.4 kcal/mol,[26] depending on the functional used, at 1/4 ML coverage and 63.0 or 64.9 kcal/mol,[27] depending on the number of metal layers, for ML coverage. These BEs are slightly higher than ours, with the difference probably due to the use of different pseudopotentials and the use of slabs with a different number of layers.

Dong and Hafner[28] report a BE (D_e) on Pd(111) of 64.3 kcal/mol for 2/3 ML, computed with ultrasoft potential. Pallassana *et al.*[29] report $D_e = 61.3$ kcal/mol at ML coverage for the same surface, using a norm conserving potential. This value increases to 63.8 kcal/mol for 1/3 ML coverage. Once again, the ultrasoft potential appears to provide larger binding energies than the more traditional norm conserving ones.

Mavrikakis and co-workers[30] report D_e for H on Ir(111) at 1/4 ML coverage in top position of 63.0 or 60.4 kcal/mol, depending on the density functional used. For the fcc site, the BE becomes 60.0 or 56.5 kcal/mol. These values are close to our computed results for 1/3 ML coverage.

Chemisorption on Pt(111) was investigated recently by Nørskov and co-workers[25] and Légaré.[31] Nørskov *et al.* report a BE with respect to gas phase H_2 of 0.25 eV/atom at 1/4 ML coverage. Depending on the reference BE for H_2, this corresponds to chemisorption energies $D_e = 60.5$ kcal/mol (using experimental H_2 BE of 4.75 eV) or 58.6 kcal/mol [using DFT H_2 BE of 4.58 eV (Ref. 23)]. Légaré reports slightly larger values: 64.1 kcal/mol at 1/4 ML coverage and 63.9 kcal/mol at ML coverage. Both sets of results are based on ultrasoft potentials and the difference between them is likely due to the use of different density functionals.

We are not aware of theoretical studies of hydrogen chemisorption on Co(001) and Os(001).

Based on the published results summarized above as well as our computations, we conclude that the effect of

TABLE IV. Interpolating functions used to fit the computed binding energies $D_0(\theta)$ in kcal/mol. These are obtained as the least squares fit of a line to the data in Table II.

Fe-bcc (110)	Co-hcp (001)	Ni-fcc (111)
$65.23 - 2.25\theta$	$61.50 - 3.30\theta$	$61.17 - 3.00\theta$
Fe-fcc (111)	Co-fcc (111)	
$66.43 - 1.65\theta$	$61.70 - 3.00\theta$	
Ru-hcp (001)	Rh-fcc (111)	Pd-fcc (111)
$63.17 - 4.35\theta$	$58.50 - 1.95\theta$	$60.07 - 3.90\theta$
Os-hcp (001)	Ir-fcc (111)	Pt-fcc (111)
$64.80 - 5.25\theta$	$60.17 - 1.50\theta$	$59.13 - 2.40\theta$

selecting different density functional theory (DFT) functionals within the GGA approximation and different ECPs may be of as large as ≈ 6 kcal/mol on the binding energies. By contrast, neglecting spin polarization may introduce errors of 1–2 kcal/mol, similar to the neglect of surface relaxation.

C. Estimate of equilibrium surface coverage

We now derive an estimate of equilibrium surface coverage from statistical thermodynamics. Although the following treatment is completely general, in the interest of readability we will provide extensive numerical examples and simulations to illustrate our results only for the case of Ir(111), limiting applications to other surfaces to coverage estimates (Figs. 5 and 6). The more complete treatment applied to Ir can easily be extended to other surfaces from the data in Table II and the expressions provided later in this document.

To estimate the equilibrium surface coverage from statistical thermodynamics, we need to make a few assumptions regarding the nature of the adsorbed hydrogen and the shape of the coverage-dependent binding energy. Some information is available from the literature regarding some of the surfaces considered, however it is likely that some surfaces may require different models. We will develop three simple models for adsorbed hydrogen that describe a variety of limiting behaviors. We find that most features observed experimentally in adsorption profiles and temperature programmed desorption (TPD) spectra can be reproduced within these models and that these results are consistent with the available surface science experiments (except for effects connected to phase changes in the adsorbate).

First we need to develop a means to interpolate the calculated binding energies over the range of coverages likely to be of interest. Experimental observations suggest that the shape of the interpolating function is not simple. Thus, for Pt and Ir, the binding energy is observed to be almost constant between 0.3 and 0.6 ML, to increase rapidly in the low coverage region and to decrease sharply approaching 1 ML[3]. Since we cannot capture such behavior by sampling the binding energy only at 1/3, 2/3, and 3/3 ML coverages and since the computed values appear to change roughly linearly with coverage up to 1 ML, we least squares fit the calculated data in Table II to a straight line. The fitting functions are reported in Table IV for all surfaces considered.
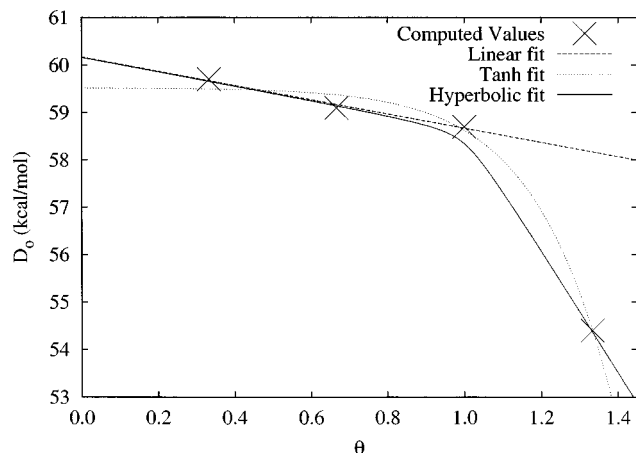
FIG. 1. Fitting functions used to interpolate the computed binding energies D_0 on Ir(111).

We now investigate for the case of iridium the effect of fitting these data to other functions and extending the fit past 1 ML coverage. We require that all interpolating functions be continuous and differentiable in the region of interest. For future reference, we refer to the linear fit of points up to 1 ML as the "linear" fit. Of course, we expect this fit to fail for coverages greater than 1 ML.

The most stable configuration with four atoms on the Ir(111) $\sqrt{3} \times \sqrt{3} R(30°)$ SUC has three atoms near top positions and one in fcc. The BE to remove the fourth atom is computed to be $D_e = 56.2$ kcal/mol. Assuming that the fourth atom in fcc position has the same zero point energy as an fcc atom at 1 ML coverage, we estimate the value $D_0 = 54.4$ kcal/mol for 4/3 ML. We can now fit a smooth function to the values at 1/3, 2/3, 3/3, and 4/3 ML as shown in Fig. 1. To assess the effect on the results since there are many plausible choices of the fitting function, we selected two rather different forms to determine how the final results are affected by this selection.

Tanh. We used a four parameter hyperbolic tangent least squares fit, namely, $D_0(\theta) = 30.05 + 29.47 \tanh(4.809 - 2.724\theta)$. We refer to this function as the "tanh" fit.

Hyperbolic. We used a hyperbole having as asymptotes the lines describing the binding energy up to 1 ML, as obtained in the linear fit, and the line connecting the points at 3/3 and 4/3 ML. The hyperbole is defined as the set of points whose distances from the two asymptotes multiplied together equal a given constant α. When the equations for the two asymptotes are $a_1\theta + b_1$ and $a_2\theta + b_2$, the hyperbole takes the form

$$D_0(\theta) = \frac{a_1\theta + b_1 + a_2\theta + b_2}{2}$$
$$- \frac{\sqrt{(a_1\theta + b_1 - a_2\theta - b_2)^2 + 4\beta}}{2}, \quad (1)$$

where $\beta = \alpha \sqrt{(1 + a_1^2)(1 + a_2^2)}$. In our particular case, the values used are (in kcal/mol) $a_1 = -1.50$, $b_1 = 60.17$, $a_2 = -12.90$, and $b_2 = 71.60$. We refer to this function as the "hyperbolic" fit. By making α small enough we can ap-

proach the linear fit in the region below 1 ML with arbitrary precision. For our modeling we chose $\alpha = 0.005$.

Figure 1 illustrates the quality of the fit obtained with the three fitting functions considered. We will find that the choice of the fitting function can affect drastically the shape of TPD spectra while leading to only minor changes in the predicted equilibrium coverage.

Several microscopic models have been proposed to mimic hydrogen chemisorption on specific metals,[4,32] but none of them is universally accepted. In very general terms, the behavior of adsorbed hydrogen must be between the two limiting cases of quantum delocalized two-dimensional gas and covalently bound site-anchored hydride. Simulations are further complicated by the presence of additional adsorbate phases depending on temperature, coverage, and which surface is being considered.

To provide a simple and intuitive description of the system, we considered three possible models for adsorbed hydrogen.

Ideal surface gas. In this model we regard the hydrogen as an ideal surface gas. Since the only interatomic interactions are through the coverage dependence of the binding energy, we expect this approach to be correct only in the low coverage and high temperature limit.

Hard-disk surface gas. This model includes the exclusion part of the intermolecular interactions. This describes saturation effects and is expected to describe correctly the behavior of most surfaces at high temperature.

Anchored. In this model each hydrogen atom is considered to be anchored to a specific surface site. This should describe the low temperature limit for surfaces having high barriers for surface diffusion.

D. Gas phase treatment

The critical parameters for gas phase hydrogen (H_2) are $T_c = 32.97$ K and $P_c = 12.76$ atm. Based on the principle of corresponding states, we expect H_2 to behave essentially like an ideal gas for temperatures greater than $2T_c(\approx 66$ K) and up to $5P_c(\approx 64$ atm). For higher pressures, deviation from ideal behavior are expected, depending on the temperature. For the scope of this study we will consider H_2 as an ideal gas.

The canonical partition function Q_g for N_g gas phase hydrogen molecules is

$$Q_g = \frac{q_g^{N_g}}{N_g!}.$$

The molecular partition function q_g includes the ZPE in the reference energy for the gas phase molecule,

$$q_g = V \frac{(2\pi m_{H_2} k_B T)^{3/2}}{h^3} \frac{1}{1 - e^{-h\nu/k_B T}} \frac{8\pi^2 I k_B T}{2h^2},$$

where ν is the vibrational frequency, I the moment of inertia, m_{H_2} the molecular mass, T the temperature, and k_B and h Boltzmann and Plank constants, respectively. The chemical potential for the gas phase is

$$\mu_g = -RT \ln(q_g / N_g). \quad (2)$$

For the computation of the partition function we used an H_2 bond distance of 0.7414 Å and a vibrational frequency of 4341 cm^{-1}.

E. Surface treatment

1. Formalism

We adopt the following formalism, common to all the approaches used to describe the adsorbed atoms. $\beta = 1/RT$; (R=gas constant); N_a is the number of adsorbed atoms; A is the surface area; ρ is the surface density (N_a/A); q_a is the partition function relative to one adsorbed atom; Q_a is the partition function relative to N_a adsorbed atoms; $[N_a]$ equals the moles of adsorbed atoms per unit area; N_s is the number of surface metal atoms; $[N_s]$ equals the moles of surface metal atoms per unit area; ν_s is the symmetric stretching frequency; q_v is $\{[1-\exp(h\nu_s/k_BT)]^{-1}\}$, the adsorbed atom vibrational partition function; θ is the surface coverage $\{[N_a]/[N_s]=N_a/N_s\}$; θ_M is the maximum possible value of θ; $E(\theta)$ is the adsorption energy relative to gas phase H_2 including zero point energy. $E(\theta)>0$ when two adsorbed atoms are more stable than one gas phase molecule at 0 K. $E(\theta)$ refers to 1 mol of adsorbed atoms; $F(\theta)$ is $[E(\theta) + \theta dE(\theta)/d\theta]$; μ_a is the chemical potential of the adsorbed atoms; and Λ is the thermal De Broglie wavelength for hydrogen $[(h^2/2\pi m_H k_B T)^{1/2}]$.

2. Quantum correction

We are interested in temperatures between 100 K, typical of surface science studies, and 800 K, typical of industrial catalysis, and in all possible values of surface coverage θ. The treatment is complicated by the fact that for an ideal Fermi-Dirac two dimensional (2D) gas at 100 K and near monolayer coverage (surface density of 0.15 molecules/Å^2) the quantum correction to the classical behavior (see derivation below) accounts for about 30% of the chemical potential. Although this correction drops to 4% at 300 K and 1 ML or at 100 K and 1/3 ML, it must be included in the statistical treatment for quantitative results to be meaningful.

The treatment of a general 2D Fermi-Dirac gas requires a number of approximations and numerical summations that would obscure the physical meaning of the resulting formulas. Hence we chose to adopt the following *ad hoc* approximate approach. We assume that the quantum correction for all the adsorption models considered here is the same as for an ideal 2D gas at the same density and temperature. This correction is added to the free energy obtained from the classical partition function. This approximation is consistent with the binding energies reported in the preceding section, which refer to a classical description of the hydrogen nuclei. This makes it questionable to correct for quantum behavior in the binding energies.

In order to proceed, we must compute the statistical free energy for an ideal 2D fermion gas in both the weakly degenerate and the classical limits.

Classical limit. We are interested in surface coverage due to the reaction

$$H_{2(g)} \rightleftharpoons 2H_a, \tag{3}$$
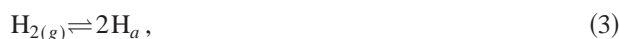
where H_a represents adsorbed atoms. The canonical partition function for N_a adsorbed atoms is

$$Q_a = \frac{q_a^{N_a}}{N_a!} e^{\beta N_a E}.$$

Since the gas is ideal, we consider constant binding energy: $E(\theta)=E$. The atomic partition function q_a contains two translational degrees of freedom,

$$q_a = A \frac{2\pi m_H k_B T}{h^2} = A/\Lambda^2. \tag{4}$$

The chemical potential in the classical limit is

$$\mu_a^{cl} = -RT\left(\frac{\partial \ln Q_a}{\partial N_a}\right)_{A,T} = RT\ln(\rho\Lambda^2) - E. \tag{5}$$

Weakly degenerate limit. The grand canonical partition function is

$$\Xi_a = \prod_k (1 + \lambda e^{-\epsilon_k/(k_BT)+\beta E}), \tag{6}$$

where $\lambda = e^{\beta\mu_a}$, the product is over all quantum states k, and ϵ_k indicates the translational energy of state k with quantum numbers n_x and n_y:

$$\epsilon_k = \frac{h^2}{8m_H A}(n_x^2 + n_y^2). \tag{7}$$

Once again we consider constant binding energy $E(\theta)=E$. The number of particles is obtained as

$$N_a = k_B T\left(\frac{\partial \ln \Xi_a}{\partial \mu_a}\right) = \sum_k \frac{\lambda e^{-\epsilon_k/(k_BT)+\beta E}}{1+\lambda e^{-\epsilon_k/(k_BT)+\beta E}}. \tag{8}$$

Notice that Eq. (8) is correct only for constant E. For large areas A, we approximate the sum with an integral over the energy by introducing the density of states for a 2D perfect gas $\omega(\epsilon)=2\pi m_H A/h^2$:

$$N_a = \frac{2\pi m_H A}{h^2}\int_0^\infty \frac{\lambda e^{-\epsilon/(k_BT)+\beta E}}{1+\lambda e^{-\epsilon/(k_BT)+\beta E}}d\epsilon$$

$$= \frac{A}{\Lambda^2}\ln(1+\lambda e^{\beta E}), \tag{9}$$

which can be solved for $\lambda = \exp(\beta\mu_a)$ and yields finally

$$\mu_a = -E + RT\ln(e^{\rho\Lambda^2} - 1). \tag{10}$$

The classical limit Eq. (5) is recovered by expanding the exponential and considering small values of $\rho\Lambda^2$:

$$\mu_a = -E + RT\ln\left[(\rho\Lambda^2) + \frac{(\rho\Lambda^2)^2}{2!} + \frac{(\rho\Lambda^2)^3}{3!} + \cdots\right]$$

$$\approx -E + RT\ln(\rho\Lambda^2). \tag{11}$$

The quantum correction is thus

$$\text{Quantum correction} = \mu_a - \mu_a^{cl} = RT\ln\left(\frac{e^{\rho\Lambda^2}-1}{\rho\Lambda^2}\right). \tag{12}$$

3. Ideal surface gas model

Since the barrier for translation parallel to the surface is generally low, we consider the case of an ideal two-dimensional surface gas. That is, we assume that adsorbed hydrogen can diffuse parallel to the surface without a barrier and that the only interatomic interactions are through the θ dependency of the binding energy. We include contributions from vibrations normal to the surface explicitly. We expect this model to fail for high values of θ, when detailed interatomic interactions become more important.

The canonical partition function is

$$Q_a = \frac{q_a^{N_a}}{N_a!} e^{\beta N_a E(\theta)}, \tag{13}$$

where the classical atomic partition function q_a is

$$q_a = A \frac{2\pi m_H k_B T}{h^2} \frac{1}{1 - e^{-h\nu_s/k_B T}} = \frac{A q_v}{\Lambda^2}. \tag{14}$$

Accordingly, the classical chemical potential is

$$\mu_a^{cl} = -RT \left(\frac{\partial \ln Q_a}{\partial N_a} \right)_{A,T}$$

$$= RT \ln\left(\frac{\rho \Lambda^2}{q_v} \right) - E(\theta) - \theta \frac{dE(\theta)}{d\theta}$$

$$= RT \ln\left(\frac{\rho \Lambda^2}{q_v} \right) - F(\theta). \tag{15}$$

Applying the quantum correction from Eq. (12), we obtain

$$\mu_a = RT \ln\left(\frac{e^{\rho \Lambda^2} - 1}{q_v} \right) - F(\theta). \tag{16}$$

The equilibrium condition obtained by equating the chemical potentials ($\mu_g = 2\mu_a$) is

$$\frac{N_g}{V} = \left(\frac{q_g}{V} \right) \left(\frac{e^{\rho \Lambda^2} - 1}{q_v} \right)^2 e^{-2\beta F(\theta)}, \tag{17}$$

and, since $\rho = \theta [N_s]$,

$$\frac{N_g}{V} = \left(\frac{q_g}{V} \right) \left(\frac{e^{\theta \Lambda^2 [N_s]} - 1}{q_v} \right)^2 e^{-2\beta F(\theta)}. \tag{18}$$

This result shows that it is not possible to define a simple (θ independent) equilibrium constant for the process. Since H_2 is ideal, the equilibrium pressure is

$$P_{H_2}^{eq} = \frac{k_B T N_g}{V} = k_B T \left(\frac{q_g}{V} \right) \left(\frac{e^{\theta \Lambda^2 [N_s]} - 1}{q_v} \right)^2 e^{-2\beta F(\theta)}. \tag{19}$$

The predicted surface coverage at any given temperature and pressure can be obtained by solving the equilibrium condition (19). However, this model contains no upper bound to the surface coverage, so that the predicted values of θ are meaningless when outside the range used to fit the θ dependence of the binding energy. This shortcoming can easily be fixed by using a fitting function that describes the sharp decrease in binding energy past monolayer coverage. This is illustrated for the case of Ir in Figs. 2(a), 2(b), and 2(c) that reports the predicted values of θ for temperatures between

100 and 800 K and selected values of pressure. Figure 2(a) contains the prediction using the linear fit from Table IV while Figs. 2(b) and 2(c) were obtained with the tanh and hyperbolic fits, respectively.

4. Hard-disk gas model

It is clear that near saturation conditions the surface hydrogen cannot be regarded as an ideal 2D gas. Since we are interested in both the low coverage and high coverage regimes, we must account for nonideal behavior of adsorbed hydrogen.

Following the approach of Van der Waals, the first correction we introduce is to assign an area to each adsorbed hydrogen. The treatment then becomes identical to the one in the preceding section for the atomic contributions to the partition function with the only difference being that the area available to each molecule depends on surface coverage. The atomic partition function q_a is thus

$$q_a = \frac{(A - bN_a)q_v}{\Lambda^2}, \tag{20}$$

where b is a parameter corresponding to the area occupied by a surface atom. To estimate b we consider that for a saturation coverage θ_M there must be no space left on the surface for further adsorption. This leads to $b = A/(N_s \theta_M)$ and hence that $b\rho = \theta/\theta_M$.

The surface canonical partition function in the classical limit is

$$Q_a = \frac{q_a^{N_a}}{N_a!} e^{N_a E(\theta)/RT},$$

from which one obtains the chemical potential in the classical limit

$$\mu_a^{cl} = -RT \ln \frac{q_a}{N_a} + RT \frac{\theta/\theta_M}{1 - \theta/\theta_M} - F(\theta)$$

$$= RT \ln\left(\frac{\rho \Lambda^2}{q_v} \right) - RT \ln(1 - \theta/\theta_M)$$

$$+ RT \frac{\theta/\theta_M}{1 - \theta/\theta_M} - F(\theta). \tag{21}$$

Applying the quantum correction from Eq. (12), we obtain the chemical potential

$$\mu_a = RT \ln\left(\frac{e^{\rho \Lambda^2} - 1}{q_v} \right) - RT \ln(1 - \theta/\theta_M)$$

$$+ RT \frac{\theta/\theta_M}{1 - \theta/\theta_M} - F(\theta). \tag{22}$$

The equilibrium condition ($\mu_g = 2\mu_a$) yields:

$$\frac{N_g}{V} = \left(\frac{q_g}{V} \right) \left(\frac{e^{\rho \Lambda^2} - 1}{q_v} \right)^2 \left(\frac{e^{\theta/(\theta_M - \theta)}}{1 - \theta/\theta_M} \right)^2 e^{-2\beta F(\theta)}. \tag{23}$$
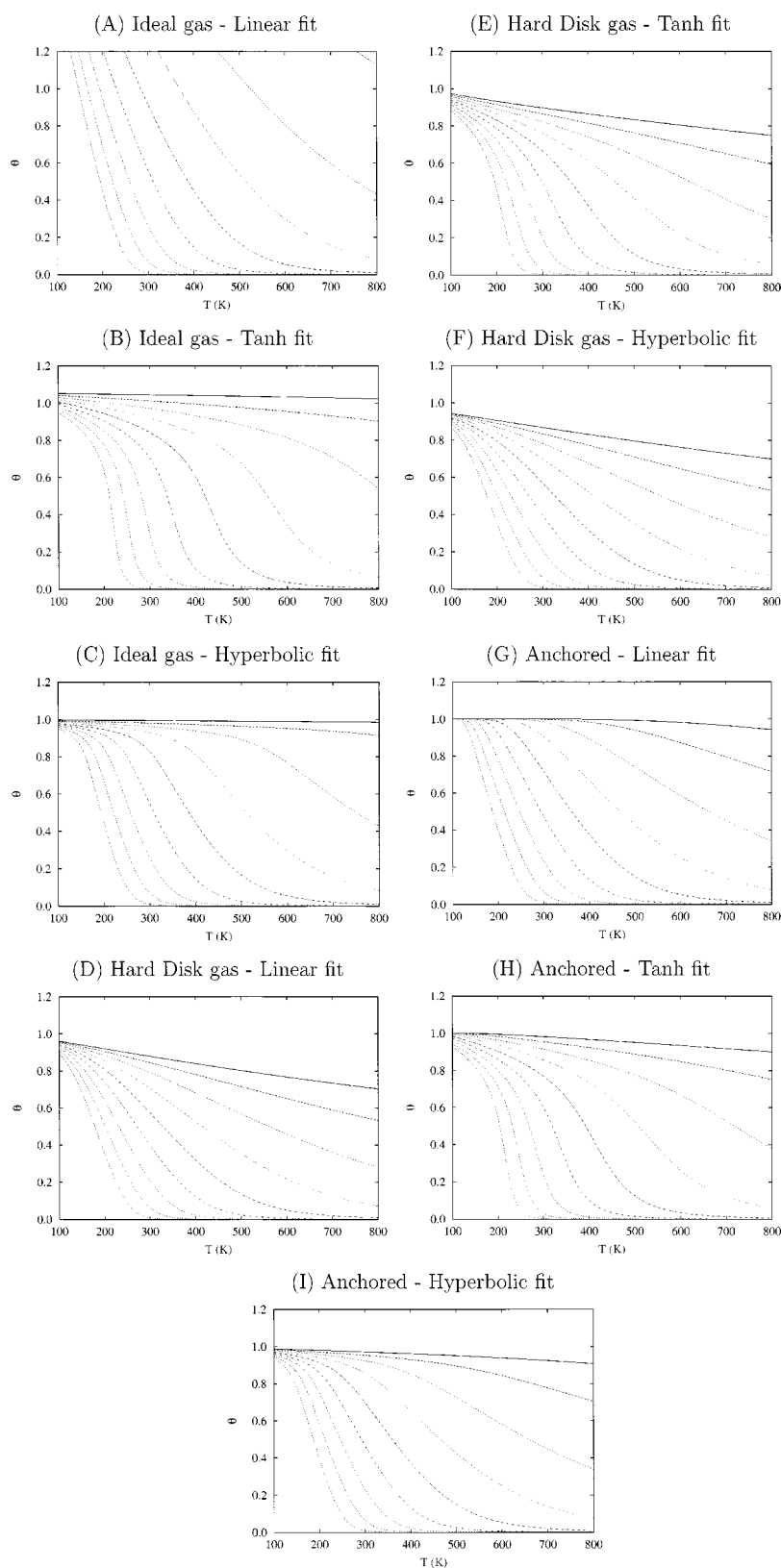
The equilibrium pressure is then

FIG. 2. Predicted equilibrium Ir(111) surface coverage θ as a function of temperature using various fits to our calculated energetics with various models. Each line corresponds to one of nine selected values of pressure: 10^{-14} (lower, leftmost line), 10^{-12}, 10^{-10}, 10^{-8}, 10^{-6}, 10^{-4}, 10^{-2}, 10^{0}, and 10^{2} atm (upper, rightmost line). All levels of approximation yield qualitatively correct coverages except for the ideal gas model using the linear interpolating function. Independent of the interpolating functions, all models behave like the ideal gas for coverages up to ≈ 0.2. We expect that real systems will exhibit behavior between the hard-disk model and the anchored model, depending on the specific system and conditions used.

$$P_{\mathrm{H}_2}^{eq} = k_B T \left(\frac{q_g}{V}\right)\left(\frac{e^{\rho\Lambda^2}-1}{q_v}\right)^2 \left(\frac{e^{\theta/(\theta_M-\theta)}}{1-\theta/\theta_M}\right)^2 e^{-2\beta F(\theta)}$$

$$= P_{id}\frac{e^{\theta/(\theta_M-\theta)}}{(1-\theta/\theta_M)^2}, \tag{24}$$

where P_{id} is the equilibrium pressure for the ideal surface gas from Eq. (19). In the special case $\theta_M=1$, the simpler form is obtained:

$$P_{\mathrm{H}_2}^{eq} = P_{id}\left[\frac{e^{\theta/(1-\theta)}}{1-\theta}\right]^2. \tag{25}$$

To determine θ_M, one obvious choice is to assume that hydrogen cannot adsorb past a monolayer coverage leading to $\theta_M=1$. This choice is consistent with the use of a linear fitting function for the binding energy. In case the fitting function has a sharp decrease in binding energy near monolayer coverage it is possible to use other values of θ_M. In particular, θ_M can be estimated as the value for which $F(\theta)=0$, i.e., the value for which an incoming H_2 molecule would experience only a repulsive potential. In the case of Ir with the tanh fit, for instance, one finds $\theta_M=1.0533$.

The predicted surface coverage at any given temperature and pressure is obtained by solving equilibrium condition (24). We report numerical solutions for the Ir(111) surface in Figs. 2(d), 2(e), and 2(f) for selected values of temperature and pressure and with the three choices of fitting function. The behavior at low coverages is similar to the one predicted with the ideal surface gas model.

5. Anchored hydrogen model

We now consider the case in which each adsorbed atom is anchored to a specific surface site. We assume there is one available site per surface metal atom and that the adsorbed atom is constrained to a 2D box of area $A/N_s\theta_M$ around the site. This corresponds to the limiting case when hydrogen atoms do not migrate on the surface even at low coverage and high temperature.

The surface partition function is

$$Q_a = \frac{q_a^{N_a}}{N_a!(N_a\theta_M-N_a)!}e^{N_aE(\theta)/RT}. \tag{26}$$

In this case the atomic partition function is

$$q_a = \frac{Aq_v}{N_s\theta_M\Lambda^2} = \frac{\theta q_v}{\theta_M\rho\Lambda^2}, \tag{27}$$

and the chemical potential in the classical limit is

$$\mu_a^{cl} = RT\ln\left(\frac{\rho\Lambda^2}{q_v}\right) + RT\ln\left(\frac{1}{1-\theta/\theta_M}\right) - F(\theta). \tag{28}$$

Applying the quantum correction we obtain

$$\mu_a = RT\ln\left(\frac{e^{\rho\Lambda^2}-1}{q_v}\right) + RT\ln\left(\frac{1}{1-\theta/\theta_M}\right) - F(\theta), \tag{29}$$

with the equilibrium condition ($\mu_g=2\mu_a$) expressed as

TABLE V. Summary of main assumptions and conclusions of the three models considered. The value $\theta_M=1$ is assumed in order to ease the comparison. $P_{id}=k_BT(q_g/V)[(e^{\rho\Lambda^2}-1)/q_v]^2e^{-2\beta F(\theta)}$.

	Ideal gas	Hard-disk gas	Anchored hydrogen
Comments	Valid in the high temperature, low barrier, low coverage limit	Valid in the high temperature, low barrier limit	Valid in the low temperature, high barrier limit
Q_a	$\dfrac{q_a^{N_a}}{N_a!}e^{\beta N_a E(\theta)}$	$\dfrac{q_a^{N_a}}{N_a!}e^{\beta N_a E(\theta)}$	$\dfrac{q_a^{N_a}}{N_a!(N_s-N_a)!}e^{\beta N_a E(\theta)}$
q_a	$\dfrac{Aq_v}{\Lambda^2}$	$\dfrac{(A-bN_a)q_v}{\Lambda^2}$	$\dfrac{Aq_v}{N_s\Lambda^2}$
$P_{\mathrm{H}_2}^{eq}$	P_{id}	$P_{id}\dfrac{e^{2\theta(1-\theta)}}{(1-\theta)^2}$	$P_{id}\dfrac{1}{(1-\theta)^2}$

$$\frac{N_g}{V} = \frac{q_g}{V}\left(\frac{e^{\rho\Lambda^2}-1}{q_v}\right)^2 \frac{1}{(1-\theta/\theta_M)^2}e^{-2\beta F(\theta)} \tag{30}$$

and the equilibrium pressure

$$P_{\mathrm{H}_2}^{eq} = k_B T\frac{q_g}{V}\left(\frac{e^{\rho\Lambda^2}-1}{q_v}\right)^2 \frac{1}{(1-\theta/\theta_M)^2}e^{-2\beta F(\theta)}$$

$$= P_{id}\frac{1}{(1-\theta/\theta_M)^2}. \tag{31}$$

Predictions on Ir for selected values of pressure are reported in Figs. 2(g), 2(h), and 2(i).

In order to ease the comparison between the models considered, we summarize the main assumptions and conclusions for the case $\theta_M=1$ in Table V. From the results reported in Fig. 2 for the Ir(111) surface it is apparent that one must include some sort of saturation to obtain a correct qualitative description of surface coverage. This can be achieved by including it explicitly in the statistical treatment, as is the case for the hard disk and the anchored models, or through the fitting function, i.e., by considering binding energies that decrease sharply for high coverages (as in the tanh and hyperbolic fits). It is also apparent that the three models predict essentially the same results for coverages under ≈ 0.2. We expect the behavior of the real system to be between the hard-disk model and the anchored model, depending on the specific system considered and the conditions used. Indeed these two models yield results that are essentially independent of the fitting function for temperatures above 400 K.

F. Adsorption and desorption

In order to predict adsorption and desorption kinetics and the time evolution of θ it is necessary to have a detailed knowledge of the transition state for the process, but we do not have this information.

Even so, we can verify that our treatment of equilibrium is consistent with available experimental data by showing that plausible assumptions about the kinetics of the process lead to adsorption profiles and TPD spectra in good agree-

ment with experiment. To this end, we derive a generic equation and investigate which assumptions must be satisfied to match the experimental observables.

We assume that the number of gas phase molecules hitting the surface per unit time is given by the equilibrium distribution of velocities, i.e., the presence of the surface does not perturb the thermal distribution in the gas phase. From transition state theory, the adsorption rate, in units of $N_g/(\text{s area})$, is

$$\text{rate}_a = S \frac{k_B T}{h} \left(\frac{2\pi m_{H_2} k_B T}{h^2} \right)^{-1/2} [H_2]$$

$$= S \left(\frac{k_B T}{2\pi m_{H_2}} \right)^{1/2} [H_2], \tag{32}$$

where S is the sticking coefficient. The desorption rate must equal the adsorption rate at equilibrium coverage, hence we must have

$$\text{rate}_d = S \left(\frac{k_B T}{2\pi m_{H_2}} \right)^{1/2} [H_2]_{eq}, \tag{33}$$

where $[H_2]_{eq}$ is the equilibrium gas concentration corresponding to surface coverage θ. In our treatment, $[H_2]_{eq} = P_{H_2}^{eq}/(k_B T)$, where $P_{H_2}^{eq}$ is given by Eqs. (19), (24), or (31). We stress the fact that $P_{H_2}^{eq}$ is the theoretical gas phase pressure required to achieve a given level of surface coverage θ under equilibrium conditions. This corresponds to a measurable hydrogen partial pressure P only in the special case that no net adsorption or desorption is under way, i.e., when the rates of adsorption and desorption are equal.

Since every adsorbed molecule results in two adsorbed atoms, the above rates must be doubled when the units of $N_a/(\text{s area})$ are used. Considering that $\theta = [N_a]/[N_s]$, we obtain the time evolution of θ described by the differential equation

$$\frac{d\theta}{dt} = S \frac{2}{[N_s]} \left(\frac{k_B T}{2\pi m_{H_2}} \right)^{1/2} \{[H_2] - [H_2]_{eq}\}. \tag{34}$$

The explicit form of Eq. (34) depends on the model used to describe $[H_2]_{eq}$ and on the sticking coefficient S.

Notice that S appears in both rate expressions. The desorption rate is expected to depend on T and θ but not on P. Therefore, S cannot depend on P or on other quantities which are functions of P, such as the equilibrium coverage. The sticking coefficient can thus depend only on T, θ, and metal specific parameters, such as the maximum coverage θ_M. Furthermore, S must be such that the rate of adsorption does not increase with coverage and the rate of desorption does not decrease with coverage. Hence, the permissible functional forms of S depend on the adopted surface model. We assume that the sticking coefficient S depends on the temperature via an Arrhenius-like expression,

$$S(T,\theta) = e^{E_A/RT} f(\theta), \tag{35}$$

where E_A is a metal dependent, temperature independent activation energy and $f(\theta)$ is a nonincreasing function of theta defined between 0 and θ_M. We further assume that the stick-

ing coefficient tends to unity in the limit of high temperature and low coverage. Therefore we impose the condition $f(0) = 1$. Based on the experimental values for the sticking coefficients, we expect E_A to be at most a couple of kcal/mol.

G. Rates using the ideal surface gas model

In the case of an ideal surface gas, rate equation (34) becomes

$$\frac{d\theta}{dt} = S \frac{2}{[N_s]} \left(\frac{k_B T}{2\pi m_{H_2}} \right)^{1/2} \left\{ [H_2] - \left(\frac{q_g}{V} \right) \right.$$

$$\left. \times \left(\frac{e^{\theta \Lambda^2 [N_s]} - 1}{q_v} \right)^2 e^{-2\beta F(\theta)} \right\}. \tag{36}$$

Since the ideal surface gas has no volume, the only plausible choice for the sticking coefficient consistent with our assumptions is $S(T,\theta) = S(T) = e^{E_A/RT}$. In particular S is constant at constant temperature. The predicted adsorption profile for Ir(111) at 100 K with linear, tanh, and hyperbolic fit is reported in Figs. 3(a), 3(b), and 3(c), where two values of S are reported for the linear fit case. In each case we compare a fit to the experimental adsorption profile.[33] It is apparent that the agreement between prediction and experiment is extremely poor for all ideal gas models, which are expected to be accurate only for values of θ tending to zero. In this regime the comparison between theory and experiment leads to an estimate for the sticking coefficient of ≈ 0.015. This value corresponds to an activation energy $E_A = 0.83$ kcal/mol.

H. Rates using the hard-disk model

In the case of hard-disk model, the kinetic equation is

$$\frac{d\theta}{dt} = S \frac{2}{[N_s]} \left(\frac{k_B T}{2\pi m_{H_2}} \right)^{1/2} \left\{ [H_2] - \left(\frac{q_g}{V} \right) \right.$$

$$\left. \times \left(\frac{e^{\rho \Lambda^2} - 1}{q_v} \right)^2 \left(\frac{e^{\theta/(\theta_M - \theta)}}{1 - \theta/\theta_M} \right)^2 e^{-2\beta F(\theta)} \right\}. \tag{37}$$

Since the surface atoms have a well defined area in this model, we expect the sticking coefficient for dissociative chemisorption to be proportional to the square of the available area, i.e, $S(T,\theta) = e^{E_A/RT}(1 - \theta/\theta_M)^2$. This functional form is acceptable since the desorption rate increases with θ and, in particular, it does not vanish for $\theta = \theta_M$. Thus we use the expression

$$\frac{d\theta}{dt} = \frac{2e^{E_A/RT}}{[N_s]} \left(\frac{k_B T}{2\pi m_{H_2}} \right)^{1/2} \left\{ (1 - \theta/\theta_M)^2 [H_2] - \left(\frac{q_g}{V} \right) \right.$$

$$\left. \times \left(\frac{e^{\rho \Lambda^2} - 1}{q_v} \right)^2 e^{2\theta/(\theta_M - \theta)} e^{-2\beta F(\theta)} \right\}. \tag{38}$$

The corresponding adsorption profile and TPD spectra are reported in Figs. 3(d), 3(e), and 3(f) and 4(d), 4(e), and 4(f).
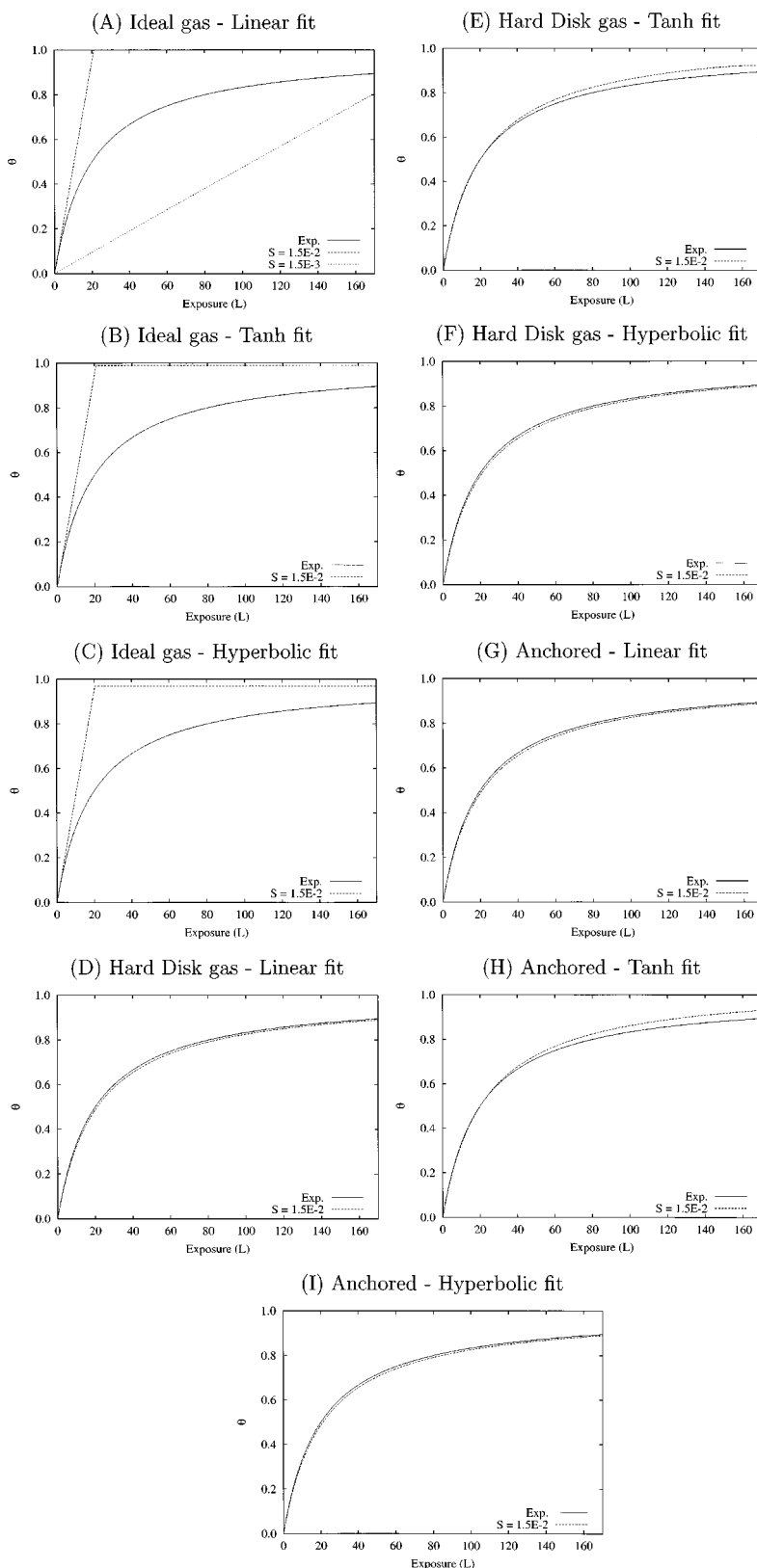
FIG. 3. Adsorption profiles on Ir(111) at 100 K computed with various statistical models and fitting functions. The solid line is a fit to experimental (Ref. 33). Exposures are in Langmuir (1 L= 1.315 79× 10^{-9} atm s). The ideal gas fails to produce the correct behavior because it does not include saturation explicitly which imposes strong constraints on the form of the sticking coefficient. The best agreement with experiment is given by the hard-disk or anchored model using the hyperbolic or linear fits.

I. Rates using the anchored model

For the anchored hydrogen model, we can use the same sticking coefficient as for the hard-disk model, resulting in the following kinetic equation:

$$\frac{d\theta}{dt} = \frac{2e^{E_A/RT}}{[N_s]}\left(\frac{k_B T}{2\pi m_{H_2}}\right)^{1/2}\left\{(1-\theta/\theta_M)^2[H_2]\right.$$
$$\left. -\frac{q_g}{V}\left(\frac{e^{\rho\Lambda^2}-1}{q_v}\right)^2 e^{-2\beta F(\theta)}\right\}. \tag{39}$$

The corresponding adsorption profiles and TPD spectra are reported in Figs. 3(g), 3(h), and 3(i) and 4(g), 4(h), and 4(i).

J. Discussion of predicted rates

Figure 3 shows that the ideal gas model cannot reproduce the experimental behavior even qualitatively. In this model the only possible form of the sticking coefficient is a constant (at constant temperature) so that the desorption rate does not decrease with coverage. In addition, as noted above for the equilibrium results, the ideal gas model fails for coverages greater than ≈ 0.2 ML.

The hard-disk and anchored models both allow more reasonable forms of the sticking coefficient and they both reproduce well the experimental curve.

Figure 4 shows that all predicted TPD spectra exhibit a shift of the peaks towards lower temperature for increasing surface coverages. This shift is quite modest for the tanh fit and much larger for both the linear and hyperbolic fits. The experimental shift between 1 and 20 L is approximately of 60 K.[34] For the same two exposures we compute shifts using the tanh fit of 33 K (anchored and ideal gas models) and 43 K (hard-disk model). The linear and hyperbolic fits are indistinguishable in this region and they yield shifts of 78 K (anchored and ideal gas models) and 91 K (hard-disk model). We predict high coverage, low temperature shoulders in the TPD spectra for all three models using the tanh fit and for all three coverage dependencies for the hard-disk gas model. We expect the shape of this shoulder to depend on the form of the fitting function used for $E(\theta)$. The TPD spectra reported in Fig. 4 refer to initial surface coverages θ between 0.02 and the saturation value for each model at a pressure of $1.315\,79\times10^{-9}$ atm. A less marked but still evident shoulder is predicted in the case of hard-disk surface gas model even when a linear fit to the binding energy is used. This indicates that the shoulder could arise from the behavior of the adsorbed hydrogen even when no weakly bound species are present.

These results show that the overall shape of the TPD spectrum is affected substantially by the surface model and fitting function used. In the case of Ir, where we expect hydrogen to diffuse extremely easily on the surface, the model that appears to best reproduce the experimental spectra is the hard-disk model with either the linear or hyperbolic fit to the binding energy. However, it is possible that different models or fitting functions might be more appropriate for other metals.

K. Surface coverage for other metals

We report in this section the predicted equilibrium surface coverages for all nine metals considered based on the hard-disk statistical model and the linear fit to the energy. Although this may not be the most appropriate combination to describe surface science experiments, in the case of high temperature catalytic processes hydrogen is expected to diffuse relatively fast on the metal surface, suggesting the hard-disk model as the most appropriate tool among those developed in this document. Furthermore, under catalytic conditions, it is customary to assume there are available sites on the surface for other species to adsorb and react. It is thus of limited interest to investigate coverages near one monolayer. Also, for intermediate coverages the adsorbed hydrogen in expected to diffuse between different adsorption sites without necessarily occupying the most stable and ordered configuration. This suggests that the linear fit to the binding energy may provide an appropriate description.

We report the estimated coverages for the surfaces stable at room temperature in Fig. 5. The unstable Fe and Co surfaces are reported in Fig. 6.

L. TPD interpretation

It is instructive to analyze the TPD spectra obtained from our simulations with the common tools used to interpret experimental TPD spectra, i.e., the generalizations of Redhead method[35] based on Polanyi–Wigner equation. Since we know the exact form of $E(\theta)$ used to produce the spectra, the values extracted from this analysis will provide an estimate of the error associated with the interpretation of experimental data.

The basic equation of the heating rate variation method for second-order desorption is

$$\ln\frac{T_M^2}{\beta} = \frac{E^\ddagger}{RT_M} + \ln\frac{E^\ddagger}{\nu R\,\theta_0}, \tag{40}$$

where T_M is the peak temperature, β is the heating rate, θ_0 is the initial surface coverage, $E^\ddagger$ is the activation energy, and ν is the preexponential factor for the Arrhenius-like kinetic equation describing the desorption process.

Consider, for instance, the behavior of Ir with the hard-disk model and the linear fit, with simulated TPD spectrum reported in Fig. 4(d). In this case, the enthalpy of adsorption for a gas phase H_2 molecule at 0 K is given by the linear fit (in kcal/mol)

$$E(\theta) = 17.1 - 3.0\,\theta. \tag{41}$$

This was obtained from the fit reported in Table IV. Since it refers to two surface atoms forming one gas phase molecule, the expression from Table IV was doubled and the bond energy of H_2 at 0 K, or 103.24 kcal/mol, was subtracted. Also, in the simulation we used an activation energy for the sticking coefficient of 0.8 kcal/mol.

We simulated the TPD spectra with heating rates of 1, 2, 5, 10, 20, and 50 K/s. For each value of initial surface coverage, we obtained the linear least squares fit to $\ln T_M^2/\beta$ versus $1/T_M$. According to Eq. (40), one can extract the values for $E^\ddagger$ and ν from the slope and the intercept. The activation energies obtained for various initial coverages are reported in
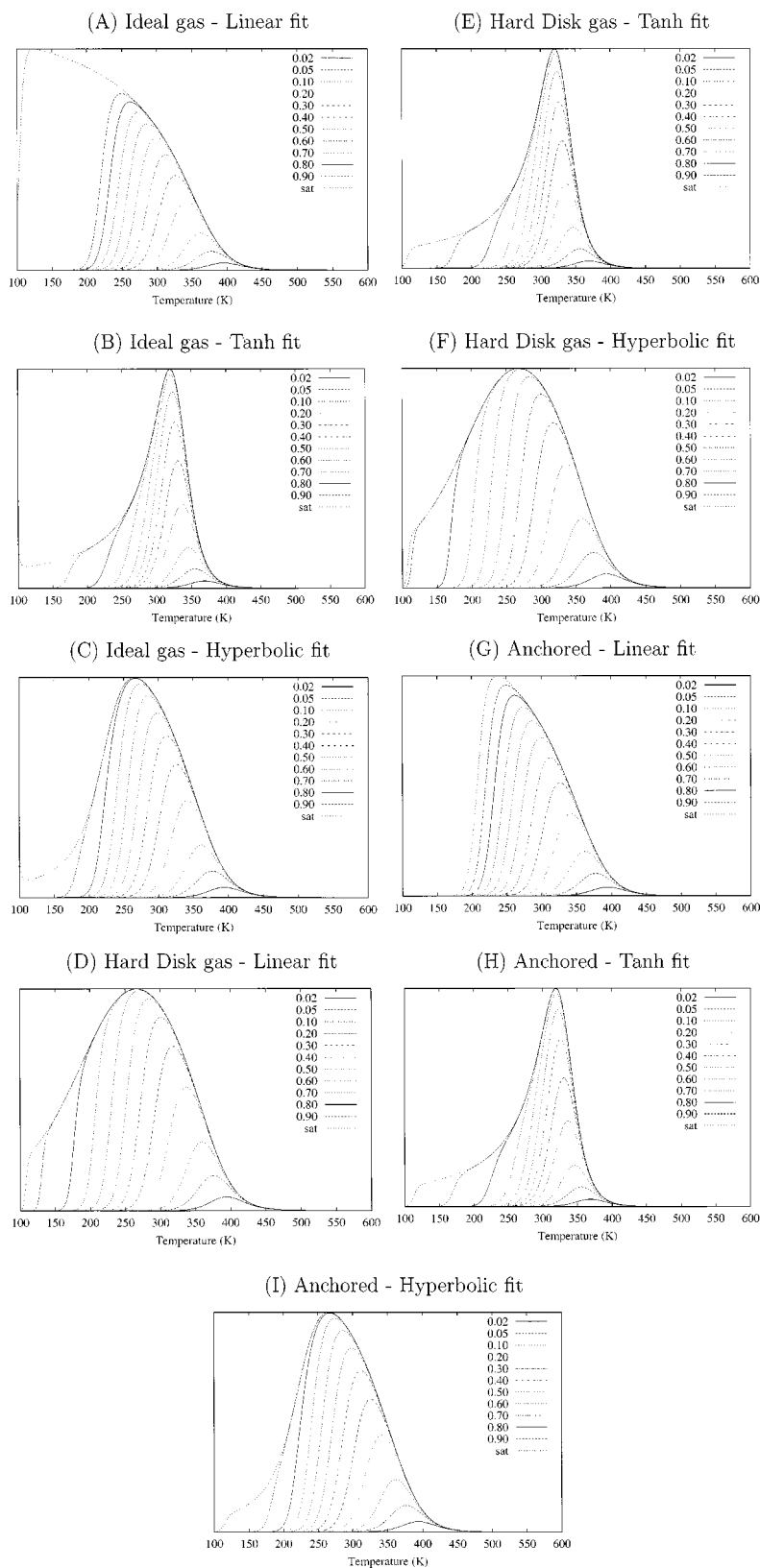
FIG. 4. TPD spectra on Ir(111) computed with various models and fitting functions. Starting coverages are in units of θ (saturation values refer to a loading pressure of $1.315\ 79\times10^{-9}$ atm). Heating rate is 20 K/s. The shape of the spectra depends on both the fitting function and the model. Thus comparison of such results with experiment can provide a criterion for selecting the model and fitting function. All nine cases lead to a single peak that shifts with increasing coverage, but the shift is smaller for the tanh fit. The hard-disk model leads to a low temperature shoulder at high coverage for all fitting functions. Probably the hard-disk model with a hyperbolic fit best compares with experiment.
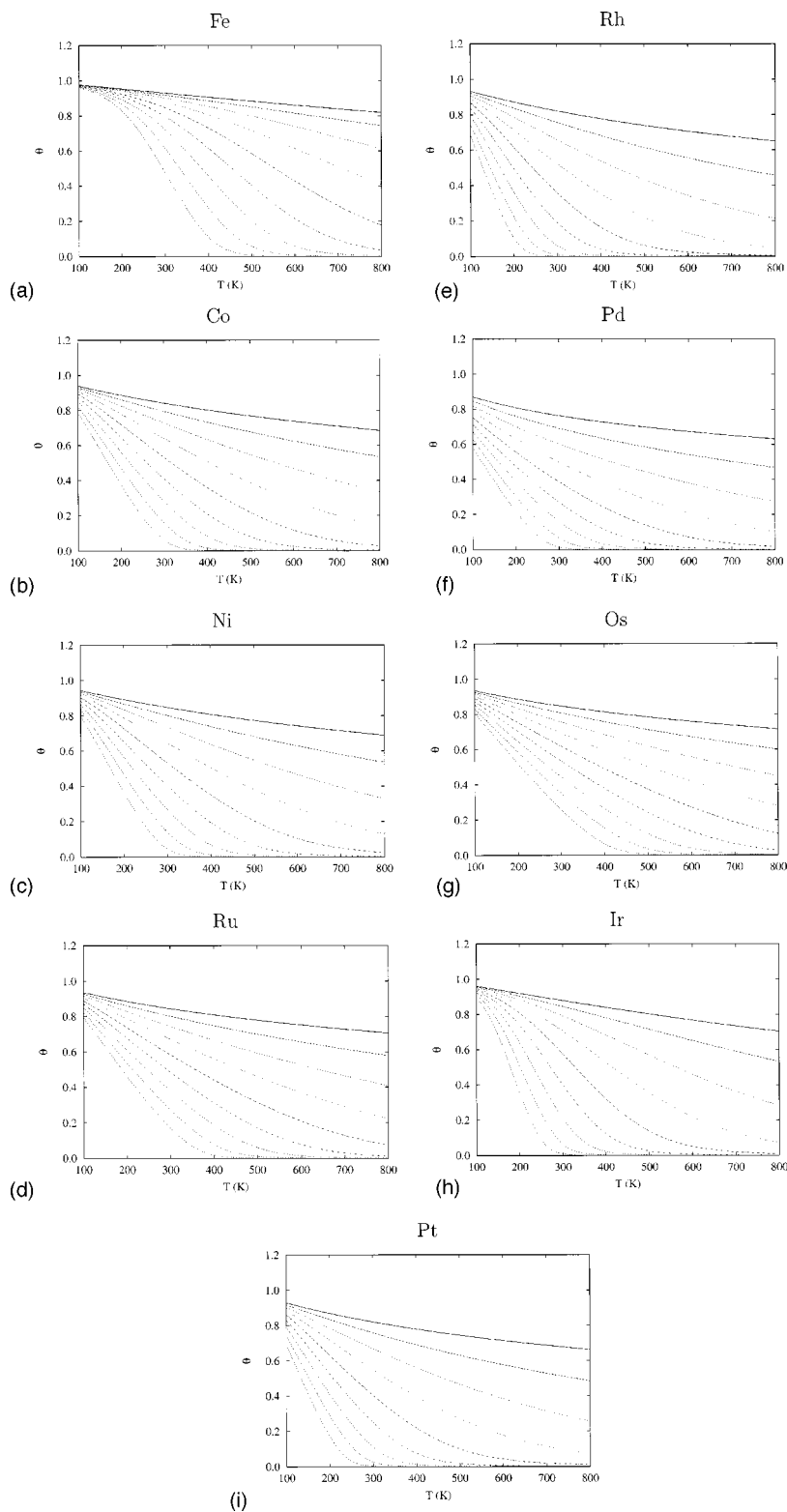
FIG. 5. Predicted equilibrium surface coverage θ for the nine stable surfaces at ambient conditions as a function of temperature using the linear fit with the hard-disk model. Each line corresponds to one of nine selected values of pressure: 10^{-14} (lower, leftmost line), 10^{-12}, 10^{-10}, 10^{-8}, 10^{-6}, 10^{-4}, 10^{-2}, 10^{0}, and 10^{2} atm (upper, rightmost line).

Table VI, where we also provide the differences between the activation energy $E^{\ddagger}$ and both the exact binding energy $E(\theta)$ and the corresponding $F(\theta) = E(\theta) + \theta dE/d\theta$. Thus we would expect $E^{\ddagger}$ at concentration θ to be related to $F(\theta)$. Indeed, for θ between 0.02 and 0.5 they differ by ≈ 1 kcal/

mol, which is close to the chemisorption activation energy of 0.8 kcal/mol which we assumed for the simulation in Fig. 4(d).

For θ greater than 0.5 the deviation in $E^{\ddagger} - F(\theta)$ increases apparently because of deviation from the Polanji–

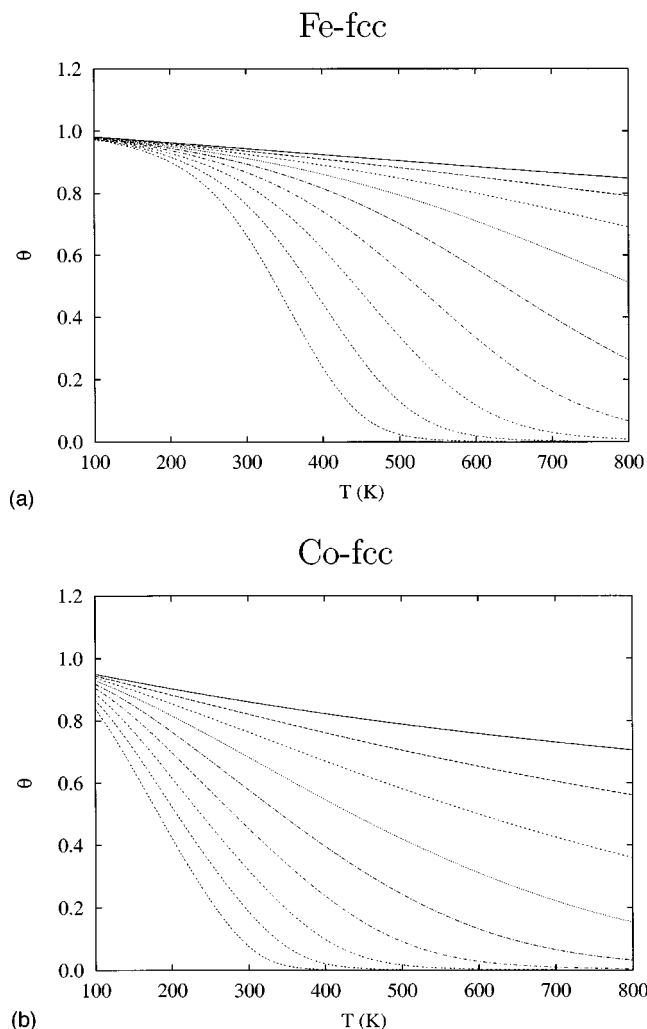## Fe-fcc

(a)

Co-fcc

(b)

FIG. 6. Predicted equilibrium surface coverage θ as a function of temperature using the linear fit with the hard-disk model. Each line corresponds to one of nine selected values of pressure: 10^{-14} (lower, leftmost line), 10^{-12}, 10^{-10}, 10^{-8}, 10^{-6}, 10^{-4}, 10^{-2}, 10^{0}, and 10^{2} atm (upper, rightmost line).

Wigner expression assumed in the Redhead analysis.

We conclude that, at least for this model of TPD which is based on equilibrium statistical thermodynamics, the commonly used interpretation methods based on the Polanji-

TABLE VI. Activation energies $E^{\ddagger}$ and preexponential factors ν obtained from the interpretation of the TPD spectra in Fig. 4(d) with a Redhead-like approach, for various initial surface coverages θ_0. The last two columns contain the difference with respect to $E(\theta)$, from Eq. (41), and $F(\theta) = E(\theta) + \theta(dE/d\theta)$.

θ_0 (ML)	$E^{\ddagger}$ (kcal/mol)	ν (ML^{-1} s^{-1})	$E^{\ddagger} - E(\theta)$ (kcal/mol)	$E^{\ddagger} - F(\theta)$ (kcal/mol)
0.02	17.9	4.8×10^{9}	0.9	0.9
0.05	17.8	5.4×10^{9}	0.8	1.0
0.10	17.5	6.0×10^{9}	0.7	1.0
0.20	16.9	7.3×10^{9}	0.4	1.0
0.30	16.4	9.8×10^{9}	0.2	1.1
0.40	15.8	1.4×10^{10}	−0.1	1.1
0.50	15.3	2.1×10^{10}	−0.3	1.2
0.60	15.1	5.4×10^{10}	−0.2	1.6
0.70	15.5	1.6×10^{11}	0.5	2.6

Wigner equation, which, in turn, is based on the Arrhenius form for the kinetics of the desorption process, provide an estimate to the function $F(\theta)$ rather than $E(\theta)$. The estimate thus obtained, however, includes the activation energy for the adsorption process. Consequently, it provides only an upper bound to the enthalpy of chemisorption. In order to extract the BE from this data, it is thus necessary to estimate the adsorption barrier.

M. Comparison with experiment

A general overview of experimental results for hydrogen adsorption on group VIII transition metals is given in several reviews.[3–5] We discuss here only published results relevant for discussing and interpreting our computations.

TPD spectra and adsorption profiles for hydrogen were obtained on Fe,[36,37] Ni,[38–41] Ru,[42–44] Rh,[45] Pd,[46,47] Ir,[19,34,48] and Pt.[49,50] All TPD spectra appear to have one peak at low coverages. The peak shifts towards lower temperatures with increasing initial exposure. This agrees with essentially all models in Fig. 4.

A second peak or shoulder appears in the low temperature region of the spectra for high initial coverages [e.g., above 150 L for Ni (Ref. 39) and above 100–160 L for Ir (Refs. 19, 34, and 48)]. Our results for the hard-disk model (all three fits) and for the tanh fit (all three surface models) lead to a pronounced shoulder in agreement with many of these results. However, we do not find the low temperature peak observed for some surfaces, namely, Fe and Ni. This peak is associated with a phase transition in the adsorbed hydrogen.[3,39,51] On other surfaces, it is associated with metal hydrides near the surface.[47] While the low temperature, high coverage phase is not likely to play any significant role in catalytic processes, it may affect significantly the surface science experiments, raising doubts on the applicability of surface science conclusions to working catalysts. In some systems, the shape of the second peak or shoulder depends strongly on the conditions used in cleaning the surface and in performing the measurement.[52]

There is general agreement that the surface binding energy depends on coverage, but there is no universally accepted model to fully interpret the TPD results. Important quantities such as binding energies and desorption barriers depend somewhat on the assumptions made in order to interpret the spectra. We suggest that the hyperbolic form might best describe both the theory and experiment.

The binding site of adsorbed hydrogen has been probed using low-energy electron diffraction (LEED), electron-energy-loss spectroscopy (EELS), and other similar techniques. Except for Ir(111) hydrogen appears to prefer three-fold cap positions on all closest packed surfaces. For Ir, there is evidence of adsorption in the top position.[19] Indeed this is consistent with our calculations which lead to a top site for Ir (by 1.4 kcal/mol) and to fcc sites for all other metals. Indeed for the $3d$ and $4d$ transition metals, the calculated binding to the top sites is too weak to dissociate H_2, while for all three $5d$ cases the top site is competitive with fcc (for Pt and Os it is 0.2 and 2.1 kcal/mol higher).

On some metals (e.g., Ir and Rh) at low surface coverage hydrogen is considered to be delocalized.[19,53]

In the low coverage region of the Ir(111) TPD spectra our results agrees well with experiments.[34] For example, an exposure of 1 L yields an experimental peak around 350 K and corresponds roughly to $\theta=0.1$, which in our TPD simulation peaks around 350 K. Also, with the linear and hyperbolic fits we predict the spectral peak close to the experimentally observed value of 250 K. We find that a low temperature shoulder in the spectra can result from saturation effects in the model or from a decreasing binding energy at high coverages. We stress the fact that the purpose of this paper is not to reliably predict TPD spectra. The agreement obtained between prediction and experiment was achieved by arbitrarily selecting the shape of the binding energy fitting function and the adsorption model. This only shows that the computed energies are consistent with the observed TPD spectra.

For other metals, other assumptions may be appropriately selected to reproduce the observed TPD spectra. For instance, the models considered so far are unable to predict a second peak in the spectra, as observed, depending on experimental conditions and sample history for Fe and Ni. A suitable modification of the fitting function may result in the appearance of two peaks in the TPD spectra.

In the case of Ni, for instance, the experimental spectra have one high temperature peak around 400 K and a low temperature peak assigned around 300 (Ref. 40) or 350 K.[41] We can reproduce these peaks assuming an activation energy for the adsorption sticking coefficient of 3.0 kcal/mol and using the following functional form for the binding energy:

$$E(\theta)=60.5-0.6\theta-0.1\tanh[10(\theta-\tfrac{1}{2})], \qquad (42)$$

which passes within the error bar of the computed values up to ML coverage. To obtain this curve, we adjusted the BE by increasing it by 0.1, 1.1, and 1.5 kcal/mol for 1/3, 2/3, and 3/3 ML coverages, respectively. We report the corresponding TPD spectrum in Fig. 7 for the hard-disk model.

Similar procedures can be applied to reproduce the main features of all other experimental spectra. Our models do not allow for phase changes in the adsorbate, which are widely believed to be responsible for the presence of multiple peaks in TPD spectra of closest packed surfaces. Also, our models are not designed to describe multilayer and subsurface adsorption, which may also affect TPD spectra by adding low temperature peaks and by changing the shape of the high temperature portion of the spectra depending on exposure and history of the sample. To describe such effects it is necessary to use more sophisticated treatments tuned to the metal of interest. However, consistency of the computed binding energies interpreted with the hard-disk and anchored models with the observed adsorption and TPD profiles, suggests that plausible assumptions can reconcile the observed spectra with our computed binding energies. We conclude as follows:

(A) The observation of low temperature shoulders does not prove the presence of two species or two phases on the surface or a stepped binding energy dependence on coverage. Of course, these effects would also result in shoulders and new peaks in the spectra. This indicates that the presence of
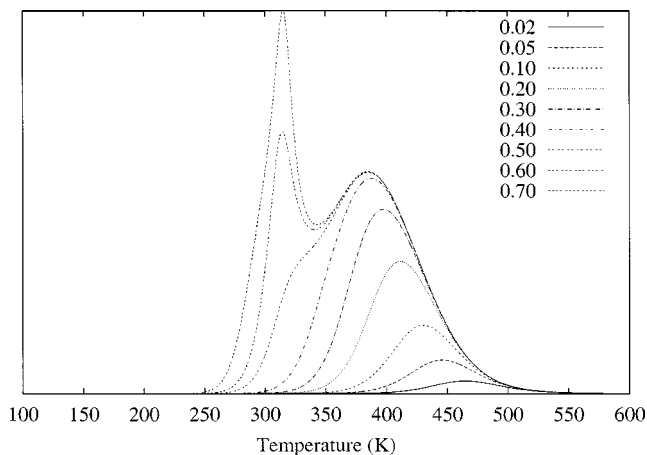

FIG. 7. Simulated TPD spectra for H_2 desorption from Ni(111). The hard-disk thermodynamics model is applied with the energy profile 42. Heating rate is 10 K/s. Each line corresponds to a different initial surface coverage as indicated in the legend.

a shoulder cannot be taken as conclusive evidence to establish the nature of adsorbed hydrogen.

(B) The computed binding energies are not in contrast with the reported TPD spectra.

All predicted equilibrium surface coverages in Fig. 2, except for the ideal gas model with linear fit, are qualitatively acceptable, but the corresponding adsorption profiles and TPD spectra differ significantly. In particular, to describe correctly the adsorption profile some form of explicit saturation effect must be included. In fact the ideal gas model provides a wrong adsorption profile even when strong interatomic interactions are included for high coverages via the binding energy dependence on θ.

V. CONCLUSIONS

We use density functional theory to investigate hydrogen coverage of the most stable surfaces of group VIII transition metals. In particular, we studied how the binding energy depends on the specific metal and surface coverage. These DFT results agree well with experimental measures with average errors of 2.0 kcal/mol in the heat of formation of adsorbed hydrogen and 6% in the vibrational frequencies. Thus the calculations match published data within experimental accuracy.

We report a simple statistical treatment of the adsorbate to validate the consistency of our results with available adsorption profiles and TPD spectra. Explicit estimates of hydrogen surface coverage at temperatures and pressures typical of catalytic conditions provide two limiting situations: high temperature with a low diffusion barrier and low temperature with a high diffusion barrier. These estimates are expected to bracket the real surface coverage.

[1] N. C. Satterfield, *Heterogeneous Catalysis in Industrial Practice* (McGraw-Hill, New York, 1991).
[2] B. C. Gates, *Catalytic Chemistry* (Wiley, New York, 1992).
[3] K. Christmann, Surf. Sci. Rep. **9**, 1 (1988).
[4] J. W. Davenport and P. J. Estrup, in *Chemisorption Systems: Part A and B*, edited by D. A. King and D. P. Woodruff (Elsevier, Amsterdam, 1990), Vol. 3, Chap. 1.
[5] G. A. Somorjai, *Introduction to Surface Chemistry and Catalysis* (Wiley-Interscience, New York, 1994).
[6] The density functional GGA is commonly known as PW91. It contains Slater local exchange (Ref. 54), Perdew-Wang '91 correlation and nonlocal exchange (Refs. 55 and 56).
[7] CASTEP, versions 3.8 and 4.2.1, as described in Ref. 57.
[8] CERIUS2, version 4.0, Molecular Simulations, Inc.
[9] J. S. Lin, A. Qteish, M. C. Payne, and V. Heine, Phys. Rev. B **43**, 4174 (1993).
[10] N. Troullier and J. L. Martins, Phys. Rev. B **43**, 1993 (1991).
[11] N. Troullier and J. L. Martins, Phys. Rev. B **43**, 8861 (1991).
[12] J. F. Paul and P. Sautet, Phys. Rev. B **53**, 8015 (1996).
[13] A. Kokalj, A. Lesar, M. Hodošček, and M. Causà, J. Phys. Chem. B **103**, 7222 (1999).
[14] D. Vanderbilt, Phys. Rev. B **41**, 7892 (1990).
[15] L. Hammer, H. Landskron, W. Nichtl-Pecher, A. Fricke, K. Heinz, and K. Müller, Phys. Rev. B **47**, 15969 (1993).
[16] W. Nichtl-Pecher, G. Gossman, L. Hammer, K. Heinz, and K. Müller, J. Vac. Sci. Technol. A **10**, 501 (1992).
[17] A. D. Johnson, K. J. Maynard, S. P. Daley, Q. Y. Yang, and S. T. Ceyer, Phys. Rev. Lett. **67**, 927 (1991).
[18] H. Yanagita, H. Fujioka, T. Aruga, N. Takagi, and M. Nishijima, Surf. Sci. **441**, 507 (1999).
[19] C. J. Hagedorn, M. J. Weiss, and W. H. Weinberg, Phys. Rev. B **60**, R14016 (1999).
[20] P. Nordlander, S. Holloway, and J. K. Nørskov, Surf. Sci. **136**, 59 (1984).
[21] D. E. Jiang and E. A. Carter, Surf. Sci. **547**, 85 (2003).
[22] J. Greeley and M. Mavrikakis, Surf. Sci. **540**, 215 (2003).
[23] G. Kresse and J. Hafner, Surf. Sci. **459**, 287 (2000).
[24] I. M. Ciobîcă, R. A. Santen, A. W. Kleyn, and J. Hafner, Chem. Phys. Lett. **311**, 185 (1999).
[25] P. Liu, A. Logadottir, and J. K. Nørskov, Electrochim. Acta **48**, 3731 (2003).
[26] M. Mavrikakis, J. Rempel, J. Greeley, L. B. Hansen, and J. K. Nørskov, J. Chem. Phys. **117**, 6737 (2002).
[27] D. X. W. Lai, Surf. Sci. **550**, 15 (2004).
[28] W. Dong and J. Hafner, Phys. Rev. B **56**, 15396 (1997).
[29] V. Pallassana, M. Neurock, L. B. Hansen, B. Hammer, and J. Nørskov, Phys. Rev. B **60**, 6146 (1999).
[30] W. P. Krekelberg, J. Greeley, and M. Mavrikakis, J. Phys. Chem. B **108**, 987 (2004).
[31] P. Légaré, Surf. Sci. **559**, 169 (2004).
[32] J. R. Engstrom and W. H. Weinberg, J. Chem. Phys. **87**, 4211 (1987).
[33] The data from Ref. 34 were fit to a second-order Langmuir model obtaining an initial probability of adsorption of 0.05 instead of the reported value of 0.0071.
[34] J. R. Engstrom, W. Tsai, and W. H. Weinberg, J. Chem. Phys. **87**, 3104 (1987).
[35] P. A. Redhead, Vacuum **12**, 203 (1962).
[36] F. Bozso, G. Ertl, M. Grunze, and M. Weiss, Appl. Surf. Sci. **1**, 103 (1977).
[37] J. Benziger and R. J. Madix, Surf. Sci. **94**, 119 (1980).
[38] K. Christmann, O. Schober, and M. Neumann, J. Chem. Phys. **60**, 4528 (1974).
[39] K. Christmann, R. J. Behm, G. Ertl, M. A. V. Hove, and W. H. Weinberg, J. Chem. Phys. **70**, 4168 (1979).
[40] R. J. Behm, G. Ertl, M. A. V. Hove, and W. H. Weinberg, J. Chem. Phys. **70**, 4168 (1979).
[41] A. Winkler and K. D. Rendulic, Surf. Sci. **118**, 19 (1982).
[42] L. R. Danielson, M. J. Dresser, E. E. Donaldson, and J. T. Dickinson, Surf. Sci. **71**, 599 (1978).
[43] H. Shimizu, K. Christmann, and G. Ertl, J. Catal. **61**, 412 (1980).
[44] R. Feulner and D. Menzel, Surf. Sci. **154**, 465 (1985).
[45] J. T. Yates, Jr., P. A. Thiel, and W. H. Weinberg, Surf. Sci. **84**, 427 (1979).
[46] H. Conrad, G. Ertl, and E. E. Latta, Surf. Sci. **41**, 435 (1974).
[47] G. E. Gdownski, T. E. Felter, and R. H. Stulen, Surf. Sci. **181**, L147 (1987).
[48] P. D. Szuromi, J. R. Engstrom, and W. H. Weinberg, J. Chem. Phys. **80**, 508 (1984).
[49] K. Christmann, G. Ertl, and T. Pignet, Surf. Sci. **54**, 365 (1976).
[50] R. W. McCabe and L. D. Schmidt, Surf. Sci. **65**, 189 (1977).
[51] R. Imbihl, R. J. Behm, K. Christmann, G. Ertl, and T. Matsushima, Surf. Sci. **117**, 257 (1982).
[52] See for instance the TPD spectra for H on Pt from Refs. 49, 50, and 3.
[53] C. M. Mate and G. A. Somorjai, Phys. Rev. B **34**, 7417 (1986).
[54] J. C. Slater, *Quantum Theory of Molecules and Solids*, The Self Consistent Field for Molecules and Solids, Vol. 4 (McGraw-Hill, New York, 1974).
[55] J. P. Perdew, in *Electronic Structure of Solids*, edited by P. Ziesche and H. Eshrig (Akademie Verlag, Berlin, 1991).
[56] J. P. Perdew, J. A. Chevary, S. H. Vosko, K. A. Jackson, M. R. Pederson, D. J. Singh, and C. Fiolahis, Phys. Rev. B **46**, 6671 (1992).
[57] V. Milman, B. Winkler, J. A. White, C. J. Pickard, M. C. Payne, E. V. Akhmatskaya, and R. H. Nobes, Int. J. Quantum Chem. **77**, 895 (2000).